Plastic Deformation Behaviour of Fe-Cu Composites

Y. Schneider[1], A. Bertram[1], T. Böhlke[2], and C. Hartig[3]

[1] Institut für Mechanik, Otto-von-Guericke-Universität Magdeburg
[2] Institut für Technische Mechanik, Universität Karlsruhe (TH)
[3] Institut für Werkstoffphysik und -technologie, TU Hamburg-Harburg

Abstract. Two-phase composites, which consist of spherical polycrystalline α-iron and copper particles, are studied mechanically under large plastic deformation. Such polycrystals are produced from mixtures of iron and copper powders by powder metallurgy. Due to the significant difference of the yield stress in the iron and the copper phase in which the slip system geometry is also dissimilar, a high heterogeneity and anisotropy characterize the plastic deformation behaviour. In such bcc-fcc polycrystals, the harder phase shows higher stresses while the softer phase undergoes a larger deformation. To successfully predict the mechanisms of the plastic deformation for a certain grain, effects of the major factors should be taken into account like, e.g., the microscopic interaction, the influence of neighbouring grains, the phase volume fraction, the morphology, and the initial crystallographic texture. In this work, an elasto-viscoplastic material model is applied in axisymmetric finite element simulations, whereas the macroscopic material behaviour is established based on constitutive equations of the single crystal. In the simulations, real two-dimensional microstructures are selected as cross-sections in the axisymmetric model. The material parameters are identified from the experimental data in compression tests. Numerical predictions include the flow behaviour, the crystallographic texture, and the local strain in Fe-Cu composites. In particular, a quantitative study is performed for the mean value of the local strain in both phases, which shows a good agreement with the experimental result for the Fe17-Cu83 composite under tension. Numerical predictions and experimental measurements are compared for the flow behaviour and the texture in both Fe17-Cu83 and Fe50-Cu50 composites.

1 Introduction

Multiphase metals are widely applicable in the automobile and aerospace industries, since they can show good ductility, enhanced strength at elevated temperature, and improved corrosion resistance. During the deformation process in such polycrystals, the microstructure and its evolution are essential for the determination of the macroscopic mechanical behaviour. The main features of the microstructure include the morphology, the arrangement, and the orientation of grains. The volume fraction of each phase and the interaction among grains are also important factors which influence the macroscopic material properties.

In such two-phase polycrystals, the harder phase shows higher stresses than the softer phase (Raabe et al. 1995; Soppa et al. 1998). To investigate the influence of local mechanical interactions among the phases on the plastic behaviour in such polycrystals, α-Fe-Cu composites as model materials have been studied in this work.

Commentz et al. (1999); Commentz (2000); Hartig and Mecking (2005) and Daymond et al. (2005) investigated for the first time the complex plastic deformation of this type of composite. Here, we introduce a mechanical approach based on finite elements to numerically study properties of iron-copper composites and compare the results with experimental data (Commentz 2000). We incorporate two-dimensional (2D) realistic morphologies, the internal interphase, and the crystallographic texture in these calculations to predict the micro- and macro-mechanical properties of Fe-Cu composites under simple tensile and compressive loads until large plastic strains.

This work is structured as following. The production of samples and processes of experimental tests are briefly introduced in Section 2. In Section 3, we summarize the constitutive equations for single crystals. The material behaviour of polycrystals is established based on the equations of the single crystal. Section 4 indicates the numerical predictions, which concern local and global deformation properties of Fe-Cu composites, and are compared with experimental results.

Notation. In the present work, 2nd- and 4th-order tensors are presented as $\boldsymbol{A}$ and $\boldsymbol{C}$, respectively. $\boldsymbol{A}^{-1}$, $\boldsymbol{A}^{\mathrm{T}}$ and $\dot{\boldsymbol{A}}$ indicate the inverse, the transpose and the material time derivative of the tensor $\boldsymbol{A}$. A linear mapping between 2nd-order tensors is written as $\boldsymbol{C}[A]$. $\boldsymbol{A} \otimes \boldsymbol{B}$ is the dyadic product of the tensors $\boldsymbol{A}$ and $\boldsymbol{B}$. $\|\boldsymbol{A}\|$ denotes the Frobenius norm of tensor $\boldsymbol{A}$.

2 Experiment

Iron-copper composites are produced from mixtures of iron and copper powders by powder metallurgy. Such powders have a purity higher than 99.9% and consist of spherical polycrystalline particles with a diameter less than 63µm. Such a production of iron-copper polycrystals follows three steps: the mixing, the pre-compression, and the final compression. The porosity of the composite is less than 1vol.%, and the samples are named after the volume fraction of the composition. Figure 1 shows the microstructure of the aforementioned Fe-Cu polycrystals (after composition) where the darker phase represents the iron. The stress-strain behaviour is studied by compressive tests which are performed on cylindrical samples (height: 9mm, diameter: 6mm) at room temperature with a constant strain rate $\dot{\varepsilon} = 10^{-4}\,s^{-1}$. The experiments have been performed by Commentz (2000). Detailed information concerning the experiment can be found in Commentz *et al.* (1999) and Commentz (2000). The $\sigma - \varepsilon$ curves are friction corrected with a friction coefficient $\mu = 0.235$. After the compression test (90% logarithmic plastic strain), the sample is ground and polished until its middle plane being parallel to the top and bottom surface is laid open. The texture measurement is accomplished on this middle surface.

Pole figures are measured for three reflections, namely {200}, {211} and {220} for the iron phase and {200} {220} {311} for the copper phase, by scanning the hexagonal grid (Matthies and Wenk 1992). The measured data are further processed in a 5×5 grid. A local resolved strain measurement is performed with a scanning electron

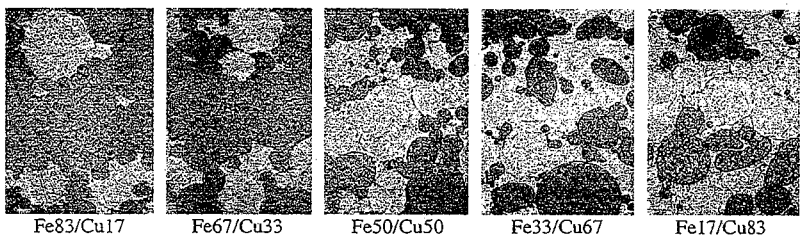

Fig. 1. Microstructures of Fe-Cu polycrystals with different phase volume fractions (Commentz 2000)

microscopic method (Commentz 2000) on a tensile sample of the Fe17-Cu83 composite. The measured cut-out is extracted from the middle plane (through the tension direction and the transverse direction) of the unloaded sample, and has a rectangular geometry with a dimension of $640\times480\mu m^2$ and $160\times120\mu m^2$ for the undeformed case and at large deformations, respectively.

3 Polycrystal Modelling

3.1 Constitutive Model

We denote the deformation gradient by $\boldsymbol{F}$. In the formulation of the elastic law, the 2nd Piola Kirchhoff stress tensor $\boldsymbol{S}$ is assumed to be a function of the right Cauchy Green tensor $\boldsymbol{C} = \boldsymbol{F}^{\mathrm{T}}\boldsymbol{F}$

$$S = \boldsymbol{h}_p(\boldsymbol{C}), \tag{1}$$

where $\boldsymbol{h}_p$ is the actual elastic law. During the plastic deformation, $\boldsymbol{h}_p$ can be related to a reference law $\boldsymbol{h}_0$ by the isomorphy condition

$$\boldsymbol{h}_p(\boldsymbol{C}) = \boldsymbol{P}\,\boldsymbol{h}_0(\boldsymbol{P}^{\mathrm{T}}\boldsymbol{C}\boldsymbol{P})\,\boldsymbol{P}^{\mathrm{T}}, \tag{2}$$

where $\boldsymbol{P}$ is the plastic transformation (Bertram 2005). $\boldsymbol{F}_e$ can be defined as

$$\boldsymbol{F}_e := \boldsymbol{F}\boldsymbol{P}. \tag{3}$$

This leads formally to the same decomposition suggested, e.g., by Lee (1969), if we identify $\boldsymbol{F}_p$ by $\boldsymbol{P}^{-1}$, i.e. $\boldsymbol{F} = \boldsymbol{F}_e\boldsymbol{F}_p$. $\boldsymbol{F}_e$ indicates the elastic distortion, the dilatation and the rotations which also accounts for rigid body rotations. $\boldsymbol{F}_p$ consists of crystallographic slips along the slip systems ($\boldsymbol{d}_\alpha$, $\boldsymbol{n}^\alpha$). The plastic incompressibility implies $\det(\boldsymbol{F}_p) = 1$. Since the elastic strains in our materials are small, we assume a linear relation between the 2nd Piola-Kirchhoff stress

$$S_e = \det(\boldsymbol{F}_e)^{-1}\,\boldsymbol{F}_e^{-1}\,\sigma\,\boldsymbol{F}_e^{-T}$$

with the Cauchy stress σ and Green's strain $\boldsymbol{E}_e^G$ in the undistorted configuration

$$S_e = \boldsymbol{C}[\boldsymbol{E}_e^G] \text{ with } \boldsymbol{E}_e^G = \frac{1}{2}(\boldsymbol{C}_e - \boldsymbol{I}) \tag{4}$$

with a (constant) elasticity tensor $\boldsymbol{C}$, the elastic right Cauchy-Green tensor $\boldsymbol{C}_e = \boldsymbol{F}_e^T \boldsymbol{F}_e$, and the 2nd-order unit tensor $\boldsymbol{I}$. A tilde indicates that a quantity is formulated with respect to the undistorted configuration which is characterized by the fact that corresponding symmetry transformations are elements of SO (3). The Kirchhoff stress tensor $\boldsymbol{\tau}^K$ is given by $\boldsymbol{\tau}^K = \boldsymbol{F}_e \boldsymbol{S}_e \boldsymbol{F}_e^T$.

The flow rule is taken from finite crystal visco-plasticity theory which specifies the time evolution of $\boldsymbol{P}$ in terms of the shear rate $\dot{\gamma}_\alpha$ and the Schmid tensors $\tilde{\boldsymbol{M}}^\alpha$ (α = 1...N). The shear rates $\dot{\gamma}_\alpha$, the Schmid resolved shear stresses τ_α, and the Schmid tensors $\tilde{\boldsymbol{M}}^\alpha$ are given as

$$\dot{\gamma}_\alpha = \dot{\gamma}_0 \operatorname{sgn}(\tau_\alpha) \left| \frac{\tau_\alpha}{\tau_\alpha^C} \right|^m , \quad \tau_\alpha = \boldsymbol{C}_e \boldsymbol{S}_e \cdot \tilde{\boldsymbol{M}}^\alpha = \boldsymbol{S}_e \cdot \tilde{\boldsymbol{M}}^\alpha ,$$

$$\tilde{\boldsymbol{M}}^\alpha = \tilde{\boldsymbol{d}}_\alpha \otimes \tilde{\boldsymbol{n}}^\alpha \tag{5}$$

respectively (Hutchinson 1976). The constant $\dot{\gamma}_0$ is the reference shear rate. A certain slip system α is specified by the slip direction $\tilde{\boldsymbol{d}}_\alpha$ and the slip plane normal $\tilde{\boldsymbol{n}}^\alpha$. For a given $\boldsymbol{L} = \dot{\boldsymbol{F}}\,\boldsymbol{F}^{-1}$, the flow rule can be formulated in terms of $\boldsymbol{F}_e$

$$\dot{\boldsymbol{F}}_e \boldsymbol{F}_e^{-1} = \boldsymbol{L} - \boldsymbol{F}_e \tilde{\boldsymbol{k}}\left(\boldsymbol{T}_e', \tau_\alpha^C\right) \boldsymbol{F}_e^{-1} ,$$

$$\tilde{\boldsymbol{k}}\left(\boldsymbol{T}_e', \tau_\alpha^C\right) = \sum_{\alpha=1}^{N} \dot{\gamma}_\alpha \left(\boldsymbol{T}_e', \tau_\alpha^C\right) \tilde{\boldsymbol{M}}^\alpha , \tag{6}$$

where $\boldsymbol{T}_e = \boldsymbol{F}_e^T \boldsymbol{\tau}^K \boldsymbol{F}_e^{-T}$ is the Mandel stress tensor. For $\boldsymbol{F}(0) = \boldsymbol{I}$, the initial condition of the differential Eq. (6) is given as $\boldsymbol{F}_e(0) = \boldsymbol{Q} \in SO(3)$, where $\boldsymbol{Q} = \boldsymbol{g}_i(0) \otimes \boldsymbol{e}_i$ is the initial orientation of the single crystal with the lattice vectors $\boldsymbol{g}_i$ and the orthonormal basis $\boldsymbol{e}_i$.

It is a reasonable assumption that the slip systems of fcc materials harden iso-tropically (Kocks and Mecking 2003) such that only one critical resolved shear stress τ^C appears in Eq. (6). For simplicity and limited by the experimental data, this concept is also applied to the iron phase of the Fe-Cu composites. Slip systems of copper and iron are chosen as <110>{111} and <111>{110} (Hartig and Mecking 2005), respectively.

The materials under consideration have been submitted to monotonous deformations (simple tension and compression) at room temperature. Under such conditions, the plastic deformation is characterized by the accumulation of dislocations in the crystal lattice. The Kocks-Mecking hardening rule, which emphasizes the mechanisms of the dislocation growth, the accumulation and the annealing is a suitable rule to be applied for materials in this work (Kocks and Mecking 2003).

The hardening rule used in the present work is

$$\dot{\tau}^C = \Theta_0 \left(1 - \frac{\tau^C}{\tau_c^v\left(\tau_\alpha, \tau^C\right)} \right) \dot{\gamma}\left(\tau_\alpha, \tau^C\right) , \quad \dot{\gamma}\left(\tau_\alpha, \tau^C\right) = \sum_{\alpha=1}^{N} \left| \dot{\gamma}_\alpha\left(\tau_\alpha, \tau^C\right) \right|$$

$$\tau_c^v = \tau_{c0}^v \left| \frac{\dot{\gamma}\left(\tau_\alpha, \tau^C\right)}{\dot{\gamma}_0^*} \right|^{\frac{1}{n}} . \tag{7}$$

In Eq. (7), Θ_0, τ_{c0}^v and $\dot{\gamma}_0^*$ are input material parameters which can be identified from experiments. N is the number of slip systems. $\dot{\gamma}_0^*$ is a material constant which is in agreement with the order of magnitude expected from the dislocation theory. n denotes the stress exponent. Detailed information on work-hardening can be found in Kocks (1976) and Kocks and Mecking (2003).

3.1.1 Homogenisation of Stresses

The above constitutive equations are suitable for a single crystal. Materials in this work are assumed to be free of pores and cracks. To describe the transition from the micro to the macro variables, we apply the representative volume element (RVE). Macro fields are determined through homogenizing the corresponding micro fields by appropriate averages over the RVE. The effective Kirchhoff stress tensor is given by the volume average over the reference volume V

$$\bar{\tau}^K = \frac{1}{V} \int_V \tau^K dV . \tag{8}$$

3.2 Finite Element Simulation

To predict the deformation behaviour of Fe-Cu polycrystals, an axisymmetric model is used in the finite element simulation which is well applicable for complex structures, inhomogeneities, and anisotropies. Here, the cross-sections of axisymmetric models are identified from the cut-outs of real microstructures, see Figure 2 and 3. In order to emphasize the interaction among the grains, the FE net is generated by the public domain software OOF (NIST, 2003). The numerical simulations are performed by ABAQUS (ABAQUS/Standard (2003)). The volume fraction of the iron phase is 22% and 49% in the simulation for the mentioned two composites. The element type applied in the simulation is CGAX3H which belongs to the generalized axisymmetric solid element of ABAQUS. Homogeneous boundary conditions are used. Schneider (2008) gives more information about the FE modelling and the applied material parameters.

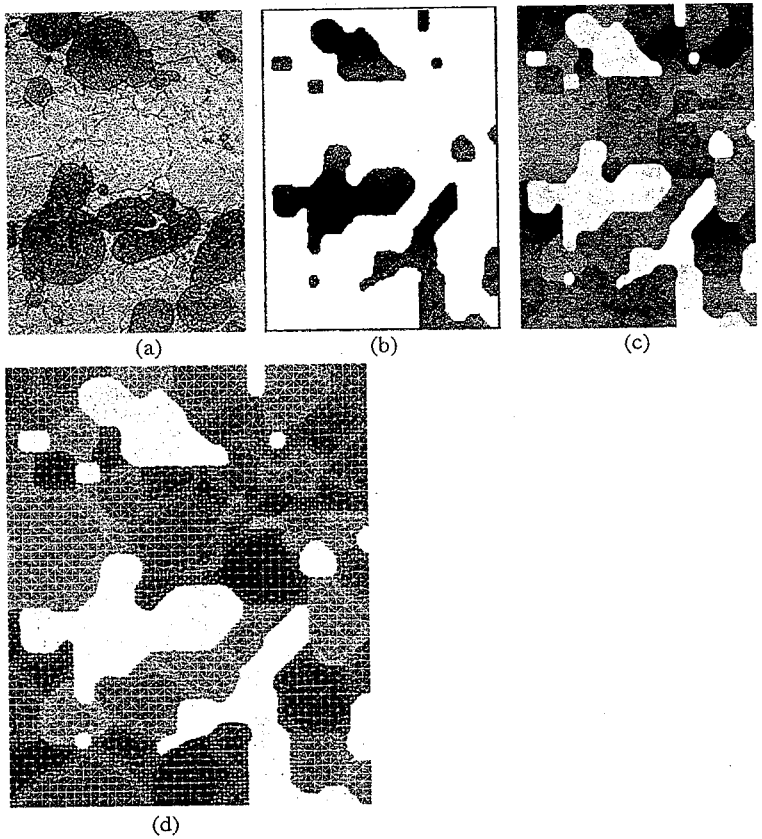

Fig. 2. Real microstructure (a), identified microstructure with the darker phase Fe (b), identified grains (c), finite element net with the refined mesh on the grain boundary (d) of the Fe17-Cu83 composite

4 Results and Discussion

4.1 Stress-Strain Flow Behaviour

Since the microscopic stress-strain behaviour can be modified by the anisotropy of the grain orientation distribution, the number of grain orientations should be representatively enough to predict the stress-strain curves which are comparable with the experimental ones.

In Figure 4, the stress-strain curve is averaged from 18 calculations with different initial grain orientations for the Fe17-Cu83 composite. Since, as already mentioned in

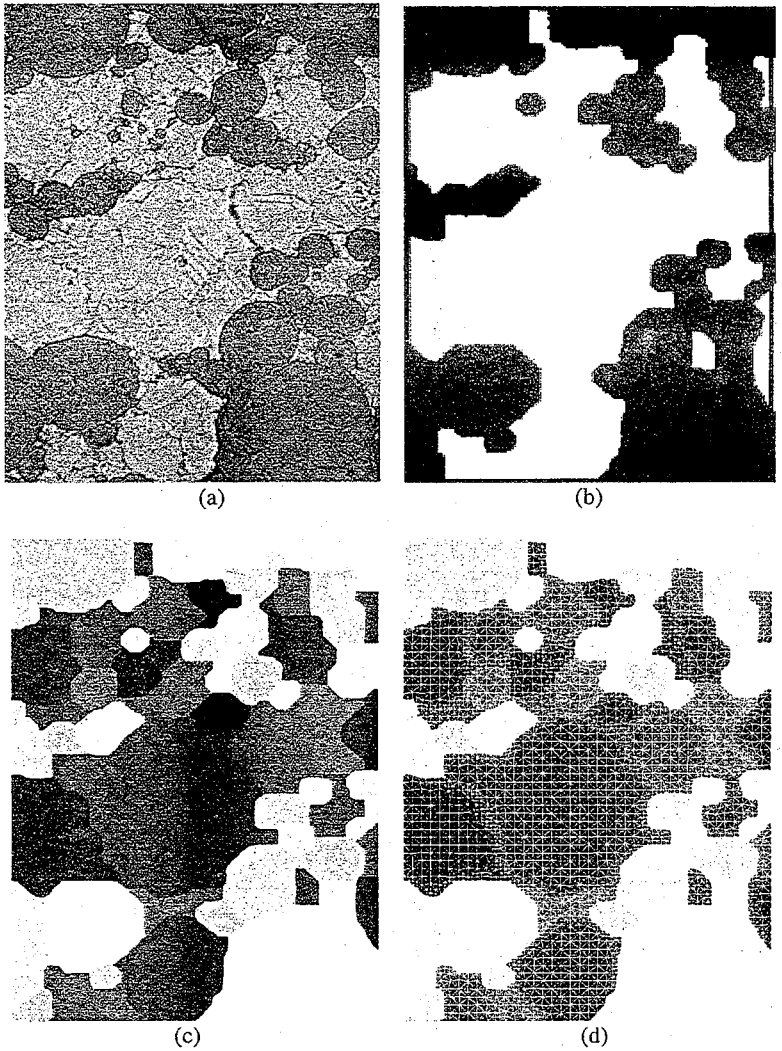

Fig. 3. Real microstructure (a), identified microstructure with darker phase Fe (b), identified grains (c), finite element net with the refined mesh on the grain boundary (d) of the Fe50-Cu50 composite

Section 3.2, the volume fraction of the Fe phase is about 22% in the axisymmetric simulation, it is reasonable that the simulated stress-strain curve is located between the experimental ones of the Fe33-Cu67 and the Fe17-Cu83 composite.

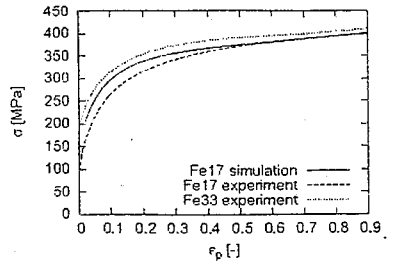

Fig. 4. Stress-strain curves of simulation and experiment for Fe17-Cu83 composite till ε_p=90% under simple compression load

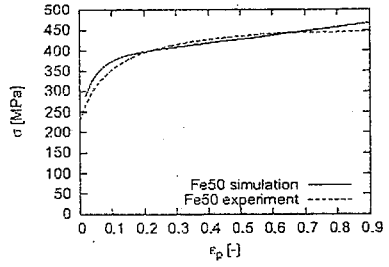

Fig. 5. Stress-strain curves of simulation and experiment for Fe50-Cu50 composite till ε_p=90% under simple compression load

Figure 5 compares the stress-strain curves of the experiment and the FE prediction which is an average of 22 simulations with different initial grain orientations. In the Fe50-Cu50 case, the simulated curve matches also well the experimental one.

In order to show the influence of the initial grain orientation on the local flow behaviour, Figure 6 and 7 exhibit the normalized stress-strain curves obtained by

$$\sigma_N = \frac{\sigma_{\max/\min}(t)}{\sigma_{\text{aver}}(t)} \quad , \quad \sigma_{\text{aver}} = \frac{\sum_{i=1}^{n} \sigma_i}{n} \tag{9}$$

with n=18 for the Fe17-Cu83 and n=22 for the Fe50-Cu50 composite.

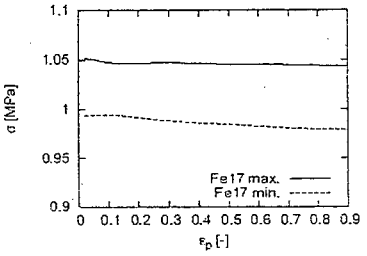

Fig. 6. Minimum and maximum stress-strain curves among 18 simulations for the Fe17-Cu83 composite; stress is normalized by averaged stress (Figure 4)

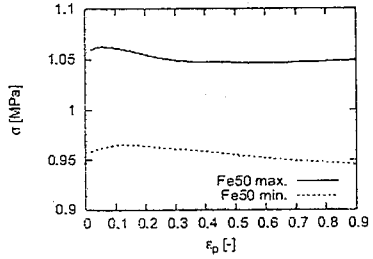

Fig. 7. Minimum and maximum stress-strain curves among 22 simulations for the Fe50-Cu50 composite; stress is normalized by averaged stress (Figure 5)

σ_N presents the normalized stress. The maximum stress and the minimum stress are given by the simulated stress-strain curves which are located at the highest and the lowest position among all the simulations, correspondingly. The deviation from the averaged stress-strain curve is about 1% to 2% for the minimum stress-strain curve (dashed line in Figure 6) of the Fe17-Cu83 composite while it is about 5% for the maximum stress-strain one. This 5% deviation remains true for the maximum and minimum stress-strain curves for the Fe50-Cu50 composite (Fig. 7).

Different orientation distributions of grains may cause 5% fluctuation for the local stress-strain curves, if a relatively small number of grains is considered in the microstructure in the axisymmetric simulation. According to Cheong and Busso (2006), such number of grains is between 10 to 100.

Fe-Cu composites exhibit an increased stiffness (compared to the pure copper) and ductility (compared to the pure iron). The phase-stress partition, i.e., the softer phase transfers the load to the harder phase, is the reason for the former property. Figure 8 and 9 show the stress flow in each phase for the Fe17-Cu83 and the Fe50-Cu50 composite, respectively. σ_{phase} and σ present the stress for the Fe or the Cu phase and the total stress, whereas both stresses are the averaged values from 3 simulations. These three simulations are chosen from the 18 (Fe17-Cu83) and the 22 (Fe50-Cu50) calculations. For a given strain, the stresses predicted by two of these 3 simulations give the largest and the smallest stress, respectively. The location of the third stress-strain curve is nearest to the averaged (stress strain) curve among the 18 (Fe17-Cu83) and the 22 (Fe50-Cu50) calculations. We define σ_{phase}/σ as the normalized phase stress. At the beginning of the yielding, the strength of the iron phase decreases fast, and that of the copper phase exhibits the reverse effect for both composites (Figure 8 and 9), whereas the rate of this decrease or increase is higher for the Fe17-Cu83 composite than for the Fe50-Cu50 composite. This trend diminishes with the increase of the plastic strain.

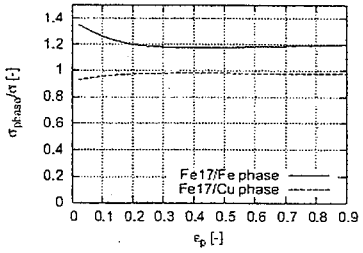

Fig. 8. Normalised stress-strain curves of Fe and Cu phases for Fe17-Cu83 composite until plastic strain ε_p=90%

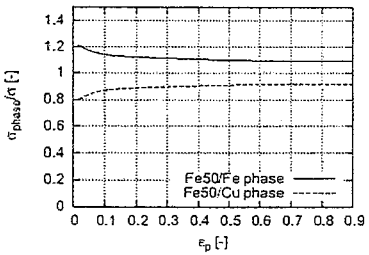

Fig. 9. Normalised stress-strain curves of Fe and Cu phases for Fe50-Cu50 composite until plastic strain ε_p=90%

At last, the normalized phase stress converges to a certain value which varies according to the ratio of (Fe:Cu) phase volume fractions. At the beginning of the yielding of the composite, it is observed that the iron phase starts to yield partly in experiments (Commentz 2000). On the other hand, some iron phase is still in the elastic-plastic transition up to higher macroscopic strains (Commentz *et al.* 1999). This means that the plastic deformation of the iron phase takes place step by step. If the harder phase yields, the load will be transferred back to the softer phase (Daymond *et al.* 2005). As a result, the stress of the iron phase decreases, while the stress of the copper phase shows the opposite effect with an increase of the plastic strain. The

observations in the experiment prove that the numerical results in Figure 8 and 9 are reasonable for the phase stress flow behaviour.

4.2 Crystallographic Texture

The crystallographic textures are presented as inverse pole figures, which are obtained from 18 and 22 calculations for Fe17-Cu83 and Fe50-Cu50 composites, respectively. The iron-phase texture presented as the standard inverse pole figure is indicated in Figure 10 for both the simulation and the experiment at 90% plastic strain under compression load.

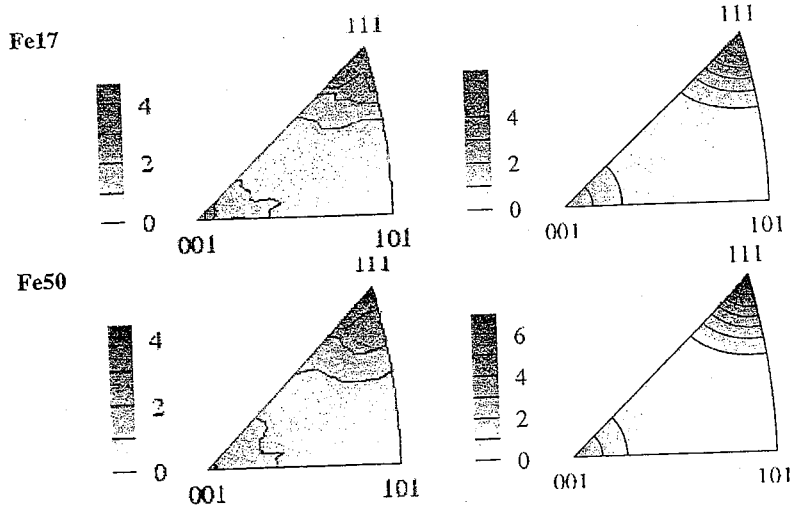

Fig. 10. Texture (inverse pole figure) of Fe phase from axisymmetric FE experiments (left) and simulations (right) at ε_p=90% for Fe17-Cu83 and Fe50-Cu50 composite

Two fibre components, <100>-fibre and <111>-fibre are observed, which are typical for compressively deformed α-Fe (Kocks *et al.* 1998). Such a fibre texture is well captured by the simulations for both the Fe17-Cu83 and the Fe50-Cu50 composite. The prediction also demonstrates the difference of the fibre intensity due to the phase volume variation, even though the maximum value of the fibre intensity is slightly higher in the Fe50-Cu50 than in the Fe17-Cu83 composite. While the experiment shows approximately the same fibre intensity. Since each inverse pole figure includes more than 600 orientations which are initially assigned randomly to the grains, the effect of the local grain orientations on the texture can be neglected. In this case, the local interaction and the phase arrangement are two major factors influencing the texture evolution in the simulation. Due to the limited number of grains in both real microstructures considered, the influence of the local interaction on the texture is a minor factor. The local morphology and the restricted confinement (homogeneous

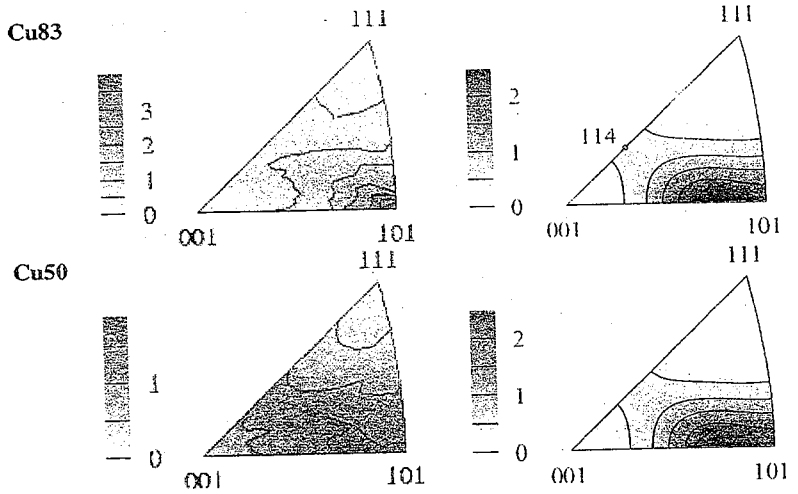

Fig. 11. Texture (inverse pole figure) of Cu phase from axisymmetric FE experiments (left) and simulations (right) ε_p=90% for Fe17-Cu83 and Fe50-Cu50 composite

boundary condition, in particular for the small cut-outs of the real microstructure) could be reasons for the sharper textures of the simulations than the real ones. The particle distribution of the Fe50-Cu50 composite may result in a higher fibre-intensity than that of the Fe17-Cu83 one, since such distributions lead to an even stiffer material structure in which four large iron particles are located on the structure boundaries.

The simulated and the experimental texture of the copper phase is given in Figure 11 for the Fe17-Cu83 and the Fe50-Cu50 composite. In the simulated textures, the pronounced <110>-fibre develops to the <411> direction. A rather soft texture of the Cu phase is presented by the measurement for the Fe50-Cu50 composite, which is not well simulated by the FE model. Besides the above mentioned reasons, i.e., the local interaction, the limited material structure, and the boundary conditions, the present model may not be able to catch the local change of the activation of the slip systems rapidly enough due to the isotropic hardening assumption.

4.3 Local Strain Distribution

The anisotropy of the constituent grains causes high heterogeneities in the local strain field when the polycrystalline structure is under load. We analysed the local strain for both the iron and the copper phase at a 19.8% tensile plastic strain. Figure 12 presents the histogram of the local plastic strain for the iron and the copper phase in the simulation (left column) and the experiment (right column, Commentz (2000)), where LD, TD, and LD/TD indicate the loading, the transverse, and the shear direction, respectively. Both the distribution and the mean value of the plastic strain match the reality well for the iron phase in all the mentioned directions. The strain of the iron phase behaves more heterogeneously in the loading direction (LD) than in the shear direction

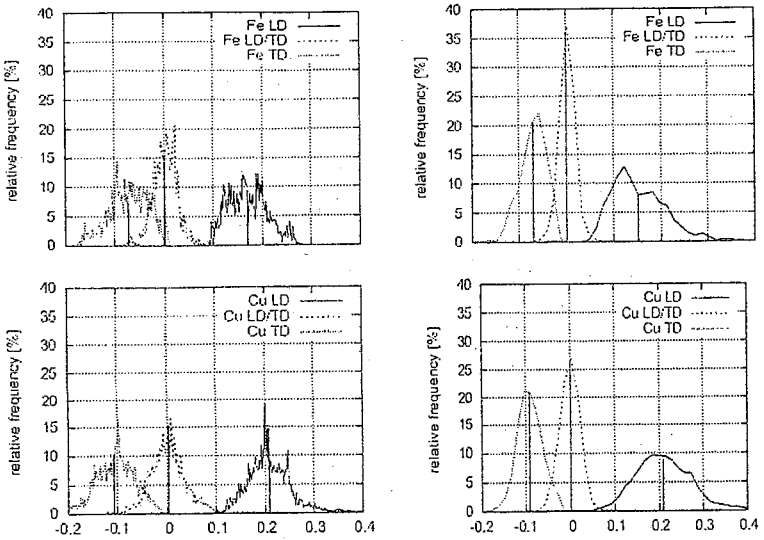

Fig. 12. Strain distribution of the Fe and the Cu phase in the axisymmetric FE simulation (left column) and the experiment (right column) for the Fe17-Cu83 composite at the tensile strain ε_p=19.8%

(LD/TD) due to the wider range and the larger oscillation of the distribution curve in the LD direction, while this non-homogeneity lies in the middle for the transverse direction (TD).

The mean value of the plastic strain is 16.99% in the loading direction for the simulation and 15.3% for the experiment. Both values are much smaller than the mean value of the composite (19.80%). These mean values are -7.1% and -7.0% for the transverse direction in the numerical and the experimental predictions, correspondingly. There is no obvious deviation of the mean value from the total one for the shear direction. Generally, the (absolute) mean value of the plastic strain for the harder iron-phase is less than that of the composite.

For the copper phase, the experiment (in Figure 12) clearly presents a wider range of the strain distribution in the loading direction than in the other two directions, i.e., there is more inhomogeneity in the LD direction. This property is well predicted by the numerical simulation. In the loading direction, the numerical curve even captures the second peak shown at approximately 27% plastic strain in the experiment. The mean value of the copper-phase plastic strain is 20.8% in the simulation and 20.9% in the experiment. The corresponding results for the TD directions are -10.6% for the FE prediction and -9.1% in the experiment, respectively. Like in the iron phase, this value is still approximately zero for the shear direction (LT/TD). Contrary to the harder phase, the mean value of the plastic strain for the Cu phase is higher than that of the total composite. This corresponds to the general conclusion for the two-phase

polycrystal mechanical behaviour, i.e., the softer phase burdens more deformation than the harder one.

5 Summary

In order to understand the mechanical behaviour of the Fe-Cu composites and, particularly, the coupling of the microscopic and the macroscopic deformation behaviour under large plastic deformations, axisymmetric simulations have been performed by the finite element software ABAQUS. The elasto-viscoplastic material model has been applied. Material structures are modelled based on real microscopic cut-outs, in which regions near grain boundaries are finer meshed than other parts. Two composites, Fe17-Cu83 and Fe50-Cu50, are taken as representative microstructures which are investigated in detail. From the investigations of the local deformation, the flow behaviour, the texture, and the distribution of the strain, we draw the following conclusions.

In the case that the local stress is influenced only by the initial grain orientations in a given microstructure, i.e., all other conditions are kept identical in the simulations, a deviation of 5% to 10% can be observed for the local stress normalized by the macroscopic stress.

The stress-strain behaviour is well captured for both Fe-Cu composites mentioned before. The stress of each phase is sensitive to the amount of the plastic deformation at the early stage of the yielding. The stress in the iron phase decreases fast, and that in the copper phase shows the reverse effect.

The simulated texture of the iron phase describes well the fibre type texture and the (maximum) fibre intensity variation according to the volume change of phases. The predicted texture of the Cu phase also captures the experimental fibre texture in the Fe17-Cu83 composite. Due to the limited number of grains in the microstructure for the simulation, the Fe50-Cu50 composite presents a higher fibre intensity than the Fe17-Cu83 composite, while no obvious difference is shown in reality.

Concerning the distribution of the plastic strain (Fe17-Cu83 composite), the mean value of the strain in both the harder phase and the softer phase presents a deviation from the total mean value in the normal and the transverse direction. The copper phase undergoes larger deformations than the iron phase in the composite. These properties are well predicted by the axisymmetric simulation.

The mean value of the strain is quantitatively well predicted for both the iron and the copper phase.

Acknowledgement. This project has been supported by the Deutsche Forschungsgemeinschaft (DFG) under the grant BE 1455/10.

References

[1] Bertram, A.: Elasticity and Plasticity of Large Deformations - an Introduction, 2nd edn. Springer, Heidelberg (2005, 2nd edn. 2008)

[2] Cheong, K., Busso, E.: Effects of lattice misorientations on strain heterogeneities in FCC polycrystals. 54, 671–689 (2006)

[3] Commentz, B.: Plastische Verformung von zweiphasigen Eisen-Kupfer-Verbundwerkstoffen. In: Dissertation. Technische Universität Hamburg-Harburg. Shaker Verlag (2006)
[4] Commentz, B., Hartig, C., Mecking, H.: Micromechanical interaction in two phase iron-copper polycrystals. Comp. Mat. Sci. 16, 237–247 (1999)
[5] Daymond, M.R., Hartig, C., Mecking, H.: Interphase and intergranular stress generation in composites exhibiting plasticity in both phases. Acta. Mater. 53, 2805–2813 (2005)
[6] Hartig, C., Mecking, H.: Finite element modelling of two-phase Fe-Cu polycrystals. Comp. Mat. Sci. 32, 370–377
[7] Hutchinson, J.: Bounds and self-consistent estimates for creep of polycrystalline materials. Proc. R. Soc. Lon. A 348, 101–127 (1976)
[8] Kocks, U.: Laws for work-hardening and low-temperature creep. J. Eng. Mater. Techn (ASME) 98, 75–85 (1976)
[9] Kocks, U., Mecking, H.: Physics and phenomenology of strain hardening: the FCC case. Progr. Mat. Sci. 48, 171–273 (2003)
[10] Kocks, U., Tome, C., Wenk, H.: Texture and Anisotropy: Preferred Orientation in Polycrystals and Their Effect on Materials Properties. Cambridge Univ. Pr., Cambridge (1998)
[11] Matthies, S., Wenk, H.: Optimization of texture measurements by pole figure coverage with hexagonal grids. Phys. Stat. Sol. (a) 133, 253–257 (1992)
[12] NIST: OOF: Object-Oriented Finite Element Analysis of Real Material Microstructures Working Group. ppm2oof1.1.24. NIST: National Institute of Standards and Technology (2003), `http://www.ctcms.nist.gov/oof`
[13] Raabe, D., Heringhaus, F., Hangen, U., Gottstein, G.: Investigation of a Cu-20 mass% Nb in situ composite Part I: fabrication. microstructure and mechanical properties. Z.Metallkd 86(6), 405–415 (1995)
[14] Schneider, Y.: Simulation of the Deformation Behaviour of Two-phase Composites. Dissertation, Fakultät für Maschinenbau, Otto-von-Guericke-Universität Magdeburg (2008)
[15] Soppa, E., Amos, D., Schmauder, S., Bischoff, E.: The influence of second phase and/or grain orientations on deformation patterns in a Ag polycrystal and in Ag/Ni composites. Comp. Mater. Sci. 13, 168–176 (1998)
[16] ABAQUS/Standard, Hibbitt, Karlsson & Sorensen, Inc. (2003)

Regularisation of the Schmid Law in Crystal Plasticity

S. Borsch[1] and M. Schurig[2]

[1] Institut für Mechanik, Otto-von-Guericke-Universität Magdeburg
[2] Federal Institute for Materials Research and Testing (BAM), Berlin

Abstract. Plastic deformations of crystals are governed by a multitude of slip systems resulting in a yield locus with corners and an irregular flow rule. To overcome these difficulties, a regularization is needed resulting in a single equation that gathers the contributions of the distinct slip systems. We investigate two complementary approaches (regularization of the yield locus, and the plastic potential, respectively). The main result is a coincidence of the approaches only for uniform slip system activity which is the case in polyslip for similar hardening states.

1 Introduction

In crystals, plastic deformation is mainly determined by dislocation movement along glide planes. The gross effect of many glide events can be modelled by the slip rates of the crystallographic slip systems. These can be seen as independently acting. Accordingly, the multi-surface theory of plasticity has been well established (Koiter 1953). It uses the formalism of the theory of plasticity for each single slip system, adding up the effect. Accordingly, a combined flow rule that contains in its symmetric and anti-symmetric parts both the plastic strain as well as the plastic spin.

In the rate-independent theory, a system of equation results, which in its solution gives the slip rates. But the decomposition of an arbitrary volume preserving deformation into a number of shear modes is in general not unique. Accordingly, this problem can be ill-posed. A solution can be found by use of a generalized inverse, see (Anand and Kothari 1996; Miehe et al. 1999; Knockaert et al. 2000).

Another solution is the adoption of a rate-dependent theory, resulting in a constitutive law for the slip rates, usually by means of a power law. The ambiguity is hereby resolved. Rate-insensitive behaviour is often modelled by a high exponent (Peirce et al. 1983; Asaro 1983; Kocks et al. 1998).

It is also possible to combine the multiple yield surfaces of the slip systems in a single yield surface of a regularized theory. Instead of using the first slip system to be active as indicator for the onset of yield (a kind of Maximum or L_∞-norm) which results in a multi-facet compound yield locus. Mollica and Srinivasa (2002) use an L_ψ-norm to combine several segments of a yield function for sheet metals into a single yield function.

Such a way has been gone independently by Gambin (1991) and Arminjon (1991). A single yield function that can be interpreted as a kind of L_ψ-norm is used, resulting in areas where more than one slip system is simultaneously active. This is not restricted to corners, like in the intersection of the slip surfaces of multiple mechanisms, but in a strict sense nearly everywhere.

Albrecht Bertram
Jürgen Tomas

Micro-Macro-Interactions

In Structured Media and Particle Systems

Springer